Water Science & Technology

Water Science & Technology Vol 84 No 9, 2601 doi: 10.2166/wst.2021.453

Re-utilization of Chinese medicinal herbal residue: waste wormwood rod-derived porous carbon as a low-cost adsorbent for methyl orange removal

Shuhui Wang[a,b], Yu Huang[b], Yiting Wu[a], Xinyu Zhang[a], Liu Wan[a], Xiang Liu[b] and Wanju Zhang[a,*]

[a] Hubei Key Lab for Processing and Application of Catalytic Materials, Huanggang Normal University, Huanggang, Hubei 438000, China
[b] Key Laboratory of Inorganic Nonmetallic Crystalline and Energy Conversion Materials, College of Materials and Chemical Engineering, Three Gorges University, Yichang, Hubei 443002, China
*Corresponding author. E-mail: wanjuzhang@126.com

XL, 0000-0002-0213-637X; WZ, 0000-0001-9219-4815

ABSTRACT

A cost-effective approach was applied to prepare porous carbon samples by the simple carbonization of wormwood rod followed by salt activator (NaCl) activation. The effect of preparation parameters on the characteristics of the wormwood rod-based porous carbons (WWRs) were studied. The properties of these samples were investigated by SEM, BET surface area, X-ray diffraction, FT-IR spectra and X-ray photoelectron spectrometer. The prepared WWRs were applied as new adsorbent materials to remove methyl orange (MO). The experimental results indicated that WWR-800 activated at 800 °C possesses the best adsorption performance. Several factors that affected the adsorption property of the system such as the solution pH, dosing of adsorbent, initial dye concentration and ionic strength were examined. In addition, the thermodynamic parameters and kinetic parameters of MO with WWR-800 were studied. The results indicated that the adsorption of MO on WWR-800 was an endothermic process and non-spontaneous under standard conditions. The maximum equilibrium adsorption capacity of MO on WWR-800 was 454.55 mg/g. After five adsorption/desorption cycles, the adsorption capacity of MO on WWR-800 remained at 94%, which indicated that wormwood rod-based porous carbon possessed good reusability.

Key words: absorption, methyl orange, porous carbon, wormwood rod

HIGHLIGHTS

- Porous carbon (WWR-800) was synthesized from waste wormwood rod by NaCl activation.
- The factors that affected the adsorption property of methyl orange on WWR-800 were systematically explored.
- WWR-800 followed the Langmuir model for methyl orange dye.
- The adsorption of MO on WWR-800 was endothermic and non-spontaneous under standard conditions.
- WWR-800 provided good reusability and stability for adsorption.

LIST OF ABBREVIATIONS

Full name	Abbreviation
Wormwood rod-0	WWR-0
Wormwood rod-600	WWR-600
Wormwood rod-700	WWR-700
Wormwood rod-800	WWR-800
Methyl orange	MO
Scanning electron microscope	SEM
X-ray diffraction	XRD
Brunauer-Emmett-Teller	BET
X-ray photoelectron spectroscopy	XPS
Nonlocal density functional theory	NLDFT
Pore size distribution	PSD
Fourier Transform infrared spectroscopy	FT-IR

1. INTRODUCTION

With the rapid development of global economy and technology in recent decades, there has been increasing demand for printing and dyeing products (Katheresan *et al.* 2018; Zereshki *et al.* 2018). Dyeing industries such as paper, rubber, plastic, leather and textile are the main sources of industrial wastewater (Wei *et al.* 2017). These wastewaters always possess high salinity, high chemical oxygen demand (COD) concentrations, and high fluctuation in pH (Alatalo *et al.* 2016). In particular, the strong coloration of the dye wastewater is one of the most important environmental concerns. The presence of dyes in the water, even at low concentration, weakens the penetration of light, which greatly hinders the photosynthesis of plants and the growth of microorganisms, leading to the deterioration of the water environment (Yang *et al.* 2013; Hu *et al.* 2014; Yu *et al.* 2017; Liu *et al.* 2019; Wang *et al.* 2019). For these above reasons, the problem of dye removal from wastewater needs to be solved urgently.

Over the past decades, many physicochemical methods, including electrochemical oxidation (Jager *et al.* 2018), membrane separation (Yu *et al.* 2017), coagulation/flocculation (Yeap *et al.* 2014), catalytic ozonation (Ghuge & Saroha 2018), filtration (Lu *et al.* 2009) and adsorption (Kim *et al.* 2018) have been investigated in the treatment of dye wastewater. Among these technologies, adsorption is preferred by researchers over other methods and widely used in wastewater treatment since it is rapid, conveniently designed and operated, impenetrable to toxic contaminants, discharges high-quality effluent and does not produce hazardous by-products (Li *et al.* 2017; Saleh *et al.* 2017; Yu *et al.* 2017; Saleh 2018; Toumi *et al.* 2018; Jain & Gogate 2019).

The efficiency of adsorption is influenced by many parameters including adsorbent, adsorbate and aqueous phase properties. Among these parameters, the type and nature of the adsorbent play a great role in the adsorption efficiency. Generally, the materials with sufficient pore volume and size, large surface area, mechanical stability, ease of regeneration, high selectivity and high adsorption capacity are acceptable and can be used as ideal adsorbents for elimination of dyes (Menya *et al.* 2018; Wong *et al.* 2018).

Activated carbon is effective and the most widely used adsorbent in the treatment of wastewater since it has outstanding capacity to absorb various chemicals (Ayranci & Duman 2009; Sun *et al.* 2018). Among them, natural biomass-derived porous carbons have attracted great attention since they are cheap and available (Mohan *et al.* 2014). The agricultural wastes, particularly lignocellulosic biomasses, have been recognized as economically-viable and sustainable sources of activated carbon (Bhatnagar *et al.* 2015). Biomass-derived porous carbons can be easily obtained by carbonization, and scholars have carried out activation treatment to optimize their adsorption effects. In generally, activation treatment can be done in two ways, namely physical (or thermal) activation and chemical activation using appropriate activators (Anfruns *et al.* 2014; Gokce & Aktas 2014; Li *et al.* 2014; Sun *et al.* 2018). Chemical activation is mostly used since it is more effective. In addition, the activation effect is tunable by adjusting the selection and dosage of activator.

Wormwood has a good reputation as a 'diamond in grass' in the plant world. It contains many trace chemical elements and minerals. It was reported that the air-dried wormwood contained 10.13% of minerals, 25.85% of proteins, and 2.59% of fat. In addition to the above components, other elements such as sodium (Na), potassium (K), magnesium (Mg), and calcium (Ca) were also found in wormwood. The pharmacological effects of wormwood are extensive, including antibacterial, antiviral, anti-oxidation, hemostasis and anticoagulant, anti-allergic, immune regulation, anti-cancer, etc (Guo *et al.* 2019; Xia *et al.* 2019). As is well known, the main medicament portion of wormwood is its leaf, while the remaining wormwood rod (WWR) is usually discarded in drug production, which inevitably becomes a serious waste and source of pollution.

In this paper, to achieve comprehensive utilization of Chinese medicinal herbal residue, waste wormwood rod was used as the carbon source to prepare porous carbon. In addition, methyl orange (MO), as one representative contamination in dye wastewater (Hui *et al.* 2018), was used as adsorbate to investigate the adsorption properties of the synthesized porous carbon materials. This study provided new insights into an environmentally friendly technique of value-added materials recovery from wormwood and its application to dye wastewater treatment.

2. EXPERIMENTAL SECTION

2.1. Chemicals

All commercial materials were used without further purification, unless indicated. The deionized water was prepared in the laboratory. Sodium chloride (NaCl), Hydrochloric acid (HCl), Sodium hydroxide (NaOH) and MO were purchased from Sinopharm Chemical Reagent Co. Ltd. Waste wormwood rod was collected from Qichun County, Hubei Province, China.

2.2. The synthesis of wormwood rod-derived porous carbons (WWRs)

The collected wormwood rod was dried at 80 °C for 60 h, smashed and screened through an 80 mesh sieve. Then the powder was put into a tube furnace by carbonization at 700 °C for 2 h with the heating rate of 5 °C min^{-1} under a continuous flow of N_2 and cooled down to room temperature. The product was washed by 1 M HCl and deionized water, filtered, and dried at 120 °C for 12 h and the black powder of WWR-0 was obtained. WWR-0 was mixed with NaCl solution at a mass ratio of 1:2 and subsequently dried at 80 °C. The dry mixtures were activated at 600 °C, 700 °C and 800 °C in N_2 for 2 h with the heating rate of 5 °C min^{-1}, respectively. The samples were stirred in 1 M HCl for 12 h and repeatedly washed by deionized water. Finally, the samples were dried in a vacuum drying oven at 120 °C and labeled as WWR-600, WWR-700 and WWR-800, respectively.

2.3. Material characterization

The surface morphology and microstructure of the WWRs samples were characterized by scanning electron microscope (SEM, Carl Zeiss Sigma 300). The crystal morphology of the WWRs samples were analyzed by the patterns of the X-ray diffraction (XRD). X-ray diffraction (XRD) analysis was conducted using an X-ray diffractometer (Shimadzu XRD-6100) in the 2θ range of 10–80° using filtered Cu Kα radiation. N_2 sorption isotherms at 77 K were tested employing a surface area analyzer (Micromeritics ASAP2020). The Brunauer-Emmett-Teller (BET) method was applied to measure specific surface area (SSA). Nonlocal density functional theory (NLDFT) method was used to calculate the pore size distribution (PSD). The functional groups on the WWRs samples were analyzed by FT-IR spectra, which were recorded using KBr with 1% of the sample at room temperature with a resolution setting of 4 cm^{-1} and 400 to 4,000 cm^{-1} range on a Nicolet MagNa-IR 6700 spectrometer. X-ray photoelectron spectroscopy (XPS) on a Thermo ESCALAB 250XI was used to analyze the chemical composition and states of samples. The binding energy of all elements was calibrated according to the C1s peak of adventitious carbon (the binding energy of C1s used for calibration was 284.8 eV). UV-Vis spectra were collected on a UV-visible spectrophotometer (TU-1901).

2.4. Adsorption experiments

Standard solutions of MO in different concentrations (1, 2, 4, 8, 16, 32 mg/L) were prepared by dissolving analytical grade MO in deionized water. To determine the adsorption capacities of WWRs samples, different amounts of the synthesized adsorbents were used in 50 mL aqueous solution containing different MO concentrations and stirred at 200 rpm in a 25 °C water bath. The solution pH was varied from 3, 5, 7, 9 and 11 using 0.1 M HCl and 0.1 M NaOH solution. The mixture was stirred for 60 min and then samples were taken and centrifuged. A spectrophotometric method was applied at 463 nm to determine the concentration of MO.

The amount of dye adsorbed on the adsorbent (q, mg/g) and removal rate (rr, %) is calculated using Equations (1) and (2), respectively (Kinoshita *et al.* 2020):

$$q = \frac{(C_0 - C_e)V}{1{,}000m} \tag{1}$$

$$rr = \frac{C_0 - C_e}{C_0} 100\% \tag{2}$$

where C_0 and C_e (mg/L) is initial mass concentration and equilibrium mass concentration, V (mL) is MO solution volume, m (mg) is adsorbent addition.

2.5. Adsorption isotherms

The dosing of adsorbent WWR-800 was 12.5 mg, the MO initial concentration was 25 to 200 mg/L with a 50 mL volume of dye solution. The solution pH was maintained at 3 using 0.1 M HCl and 0.1 M NaOH solution. The solutions were stirred at 200 rpm in a 25 °C water bath for 60 min. The aliquot of MO was analyzed by UV-Visible Spectroscopy at the wavelength of 463 nm.

2.6. Regeneration

After every adsorption cycle, the WWR-800 was regenerated by the same method. Firstly, the adsorbent and dye solution were separated by filtration device, and then hydrochloric acid (1 M HCl) was added to soak for 60 min under ultrasonic conditions. After the hydrochloric acid and the adsorbent were separated by filtration device, distilled water was added to

wash until pH = 7. Finally, the adsorbent was dried in a vacuum oven at 120 °C for 12 h. The regenerated WWR-800 was employed for 5 cycles of the adsorption-desorption of MO under 25 °C to check its reusability and stability. Reusability was investigated with 25 mg (0.5 g/L) of the adsorbent in 50 mL of 50 mg/L of MO initial concentration solutions at pH 3 and stirred at 200 rpm. The aliquot was tested by using UV-Visible Spectroscopy after 60 min.

3. RESULTS AND DISCUSSION

3.1. Morphology characterization of WWRs

In this study, WWRs samples were prepared by carbonizing wormwood rod followed by NaCl activation. It was found that the NaCl activation plays an important role in the development of the pore structure in WWRs samples. In particular, the surface area and the pore structure of the WWRs samples were influenced by the activating temperature to the pre-carbonization samples. The SEM images (Figure 1) show that with increasing of activating temperature, the WWRs sample had obvious tube-like structure and a large amount of meso/macropores, which might be caused by the NaCl as a water-soluble template (Qian *et al.* 2015; Wang *et al.* 2016; Gao *et al.* 2020).

3.2. Structure characterization of WWRs

The XRD patterns of WWR-0, WWR-600, WWR-700, and WWR-800 were shown in Figure 2(a). There existed two diffraction peaks around 23° and 43° for all samples, which can be assigned to (002) and (100) crystallographic planes of the disordered carbon layer, respectively. The broad peak at 23° with low intensity suggested an amorphous structure. While another low

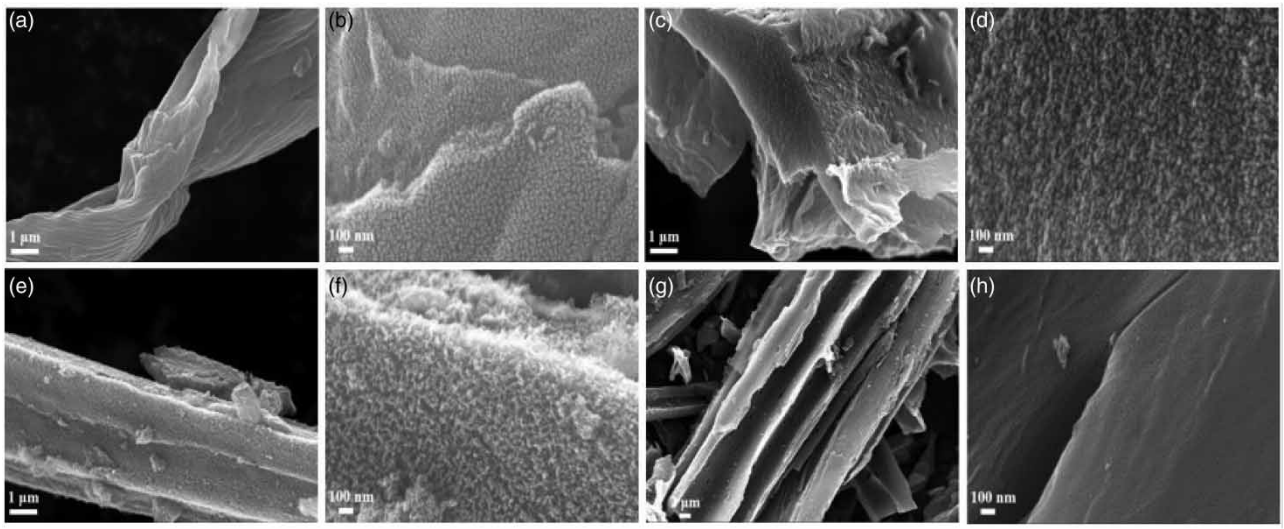

Figure 1 | SEM images of (a, b) WWR-0; (c, d) WWR-600; (e, f) WWR-700; (g, h) WWR-800.

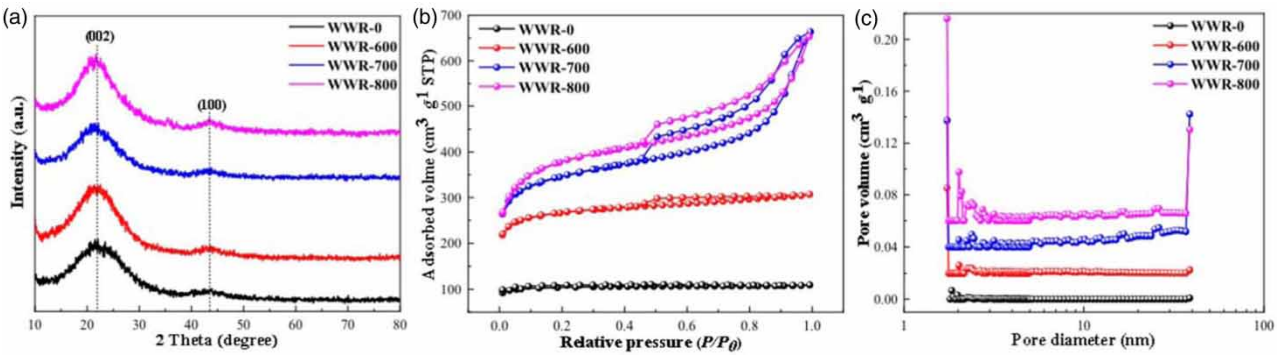

Figure 2 | (a) XRD patterns; (b) N_2 adsorption-desorption isotherm; (c) pore size distribution of WWR-800.

diffraction peak intensity at 43° indicated the formation of graphitic structure (Wang *et al.* 2018). With the increase of activation temperature, the 23° diffraction peak gradually increased, indicating that the degree of amorphous structure gradually increased. Furthermore, there was no detection of signals ascribable to other species, implying complete removal of NaCl species.

As shown in Figure 2(b), WWR-0 had some micropores and belonged to the type I isotherm. WWR-600, WWR-700, and WWR-800 showed the combined characteristics of type IV isotherms with a hysteresis loop. Among them, WWR-800 possessed an ultrahigh N_2 adsorption capacity. The dramatic increase in the volume adsorbed at a relative pressure <0.05 indicated the existence of a great number of micropores. The observation of the hysteresis loop resulting from the high capillary effect at a relative pressure in the range of 0.4–0.8 suggested the presence of a mesopore structure. Moreover, the increase at a relative pressure >0.8 demonstrated the presence of a number of macropores. Additionally, the pore size distribution in Figure 2(c) also revealed the microporous and mesoporous structures with the presence of macropores. Thus, the hierarchical porous carbon material was successfully synthesized, which benefited the fast adsorption and diffusion/transportation of adsorbate molecules (Cazetta *et al.* 2016; Yao *et al.* 2018). Consequently, WWR-800 was confirmed to possess the highest surface area of 1,242.25 m^2/g in all samples (Table 1). Overall, WWR-800 had a high surface area and 3D architecture with multiconnected micro/meso/macropores with proper pore size distribution. This may be due to the addition of the activator NaCl and activation at a high temperature of 800 °C. NaCl served as a water-soluble template for macropores, while micropores and mesopores were formed by the reaction of carbonized products with CO_2 and the intercalation of NaCl (Qian *et al.* 2015; Zhang *et al.* 2019).

3.3. Chemical composition of WWR-800

Our purpose was to explore the wormwood rod-derived porous carbon with best adsorption property, so the surface analyses of WWR-800, which had the highest surface area of the prepared WWRs, was further obtained by XPS measurement. Figure 3(a) shows the XPS survey spectrum of WWR-800, of which the peaks at around 284.8 eV, 400.1 eV and 533.0 eV correspond to C1s, N1s and O1s, respectively. As shown in the C1s spectra (Figure 3(b)), the predominant surface functional group of WWR-800 was graphitic or amorphous C (C-1, around 284.8 eV, 75.42%), the sp^2-type carbon C (C-2, such as -C = N groups, carbon in phenolic, alcohol or ether, 285.5 eV, 0.02%), the sp^3-type carbon C (C-3, such as C = N bonding states, carbon in carbonyl or quinone groups, around 286.3 eV, 18.03%), and the carboxyl carbon (C-4, centered at 288.5 eV, 6.53%), respectively. N1s spectrum can be resolved into four peaks (Figure 3(c)). Two of the biggest peaks, around 398.6 eV (15.89%) and 400.1 eV (49.92%), were assigned to the pyridinic N (N-1) and pyrrolic/pyridone N (N-2), respectively. The peak around 401.4 eV (1.72%) and 402.0 eV (32.47%) can be subsumed to quaternary N (N-3) and oxidized N (N-4), respectively. As displayed in Figure 3(d), the four peaks fitted in the O1s spectra can be assigned to highly conjugated forms of phenolic O (O-1, 530.9 eV, 0.63%), the unsaturated carbon-oxygen single bond (lactone, ether-like or anhydride, O-2, 532.0 eV, 95.11%), the carbon-oxygen double bond (O-3, 533.0 eV, 2.98%) and carbonyl oxygen (such as quinone or pyridone groups, O-4, 533.8 eV, 1.29%), respectively. These oxygenous and nitrogenous groups were expected to contribute to the hydrophilic dye adsorptions (Ge *et al.* 2015; Zhao *et al.* 2021).

3.4. Adsorption experiment studies

3.4.1. Effect of solution pH

A constant amount (12.5 mg) of WWRs were added in 50 mL MO dye solutions (50 mg/L), then the mixtures were stirred at 200 rpm in a 25 °C water bath for 120 min. The adsorption properties of WWRs on MO are shown in Figure 4. It can be seen from the figure that the adsorption reached equilibrium state within 60 min in all curves. The results indicated that the

Table 1 | Pore parameters of WWRs samples

Samples	S_{BET} ($m^2\ g^{-1}$)	S_{micro} ($m^2\ g^{-1}$)	V_{total} ($cm^3\ g^{-1}$)	V_{micro} ($cm^3\ g^{-1}$)
WWR-0	336.72	296.67	0.28	0.14
WWR-600	865.42	666.00	0.77	0.32
WWR-700	1,141.83	731.77	1.26	0.35
WWR-800	1,242.25	711.82	1.09	0.35

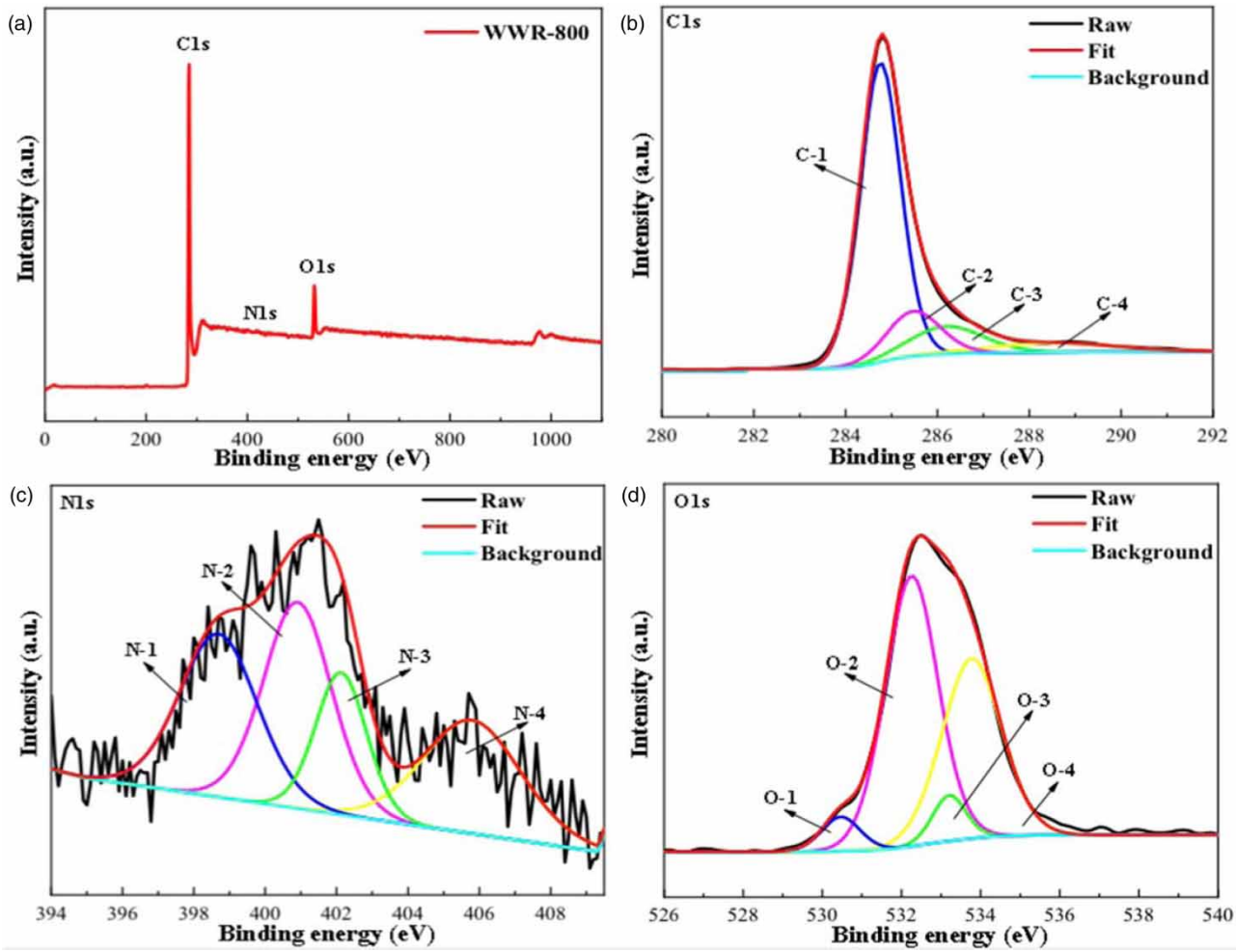

Figure 3 | (a) XPS spectra of WWR-800 and high-resolution XPS survey of (b) C1s; (c) N1s and (d) O1s.

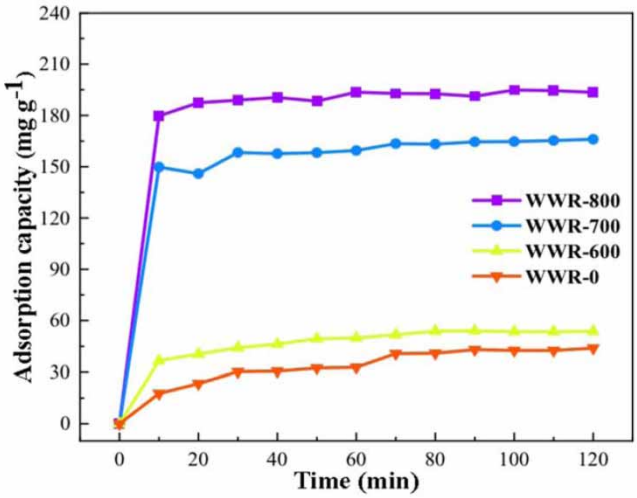

Figure 4 | Adsorption performance of WWRs: 50 mg/L of MO, 12.5 mg (0.25 g/L) of WWRs, 25 °C.

adsorption capacity of WWRs for MO is WWR-800 > WWR-700 > WWR-600 > WWR-0. Hence, WWR-800 was chosen as the optimal adsorbent for further adsorption study.

The solution pH is a significant parameter in the dye adsorption process since it can alter the surface charge of the adsorbent and the structure of the dye molecules (Azam *et al.* 2020). A constant amount (12.5 mg) of adsorbents were added in 50 mL MO dye solutions (50 mg/L) of pH 3, 5, 7, 9, and 11. Figure 5(a) shows the results obtained by the WWR-800 at different pH MO solutions. It was deduced from the figure that the MO adsorption onto WWR-800 was strongly pH-dependent. Adsorption of MO decreased with an increase in pH value. At this lower pH, a considerable high electrostatic attraction existed between the positively charged surface of the adsorbent and anionic MO species. The pK_a of MO was 3.46, indicated that the MO molecule existed as negatively charged species when the solution pH was 3.0. Until pH = 3.46 afterwards MO existed as neutral and in high pH conditions as slightly positive charged species. Thus, with the pH increased, a growing number of OH^- caused repulsion between the negatively charged surface and the dye molecules (Subbaiah & Kim 2016).

3.4.2. Effect of initial dye concentration

To investigate the effect of dye concentration on the adsorption process, different concentrations of MO aqueous solution (25–200 mg/L) were used. The dosing of the adsorbent (WWR-800) was 12.5 mg per 50 mL of dye solution at pH 3. The results obtained after 60 min adsorption are shown in Figure 5(b). WWR-800 adsorption capacity increased linearly with the initial mass concentration of MO, while the removal rate decreased gradually. The reason was that when the initial mass concentration of MO increased, the driving force caused by the existence of pressure gradient also increased, which made more MO molecules move to the adsorption site (Khanday & Hameed 2018). The adsorbed amount of MO increased from 196.34 mg/g to 607.08 mg/g as the initial concentration was enhanced from 25 mg/L to 200 mg/L, indicating that removal performance was affected by the initial concentration of MO.

3.4.3. Effect of dosing of adsorbent

To study the effect of adsorbent dosage on the adsorption process, different amounts (12.5, 25, and 37.5 mg) of WWR-800 were added in 50 mL of 50 mg/L MO and stirred at 200 rpm in a 25 °C water bath. Figure 5(c) shows the results obtained after adsorption of 60 min. The removal efficiency of MO increased as the dose of WWR-800 increased in low adsorbent dose. When the dose of WWR-800 was 12.5 mg (0.25 g/L), the removal efficiency and adsorption capacity were 96.62% and 193.58 mg/g, respectively. When the adsorbent dose continuously increased to 0.5 and 0.75 g/L, the removal efficiency gradually tended to be flat. On the contrary, the adsorption capacity decreased due to the adsorption site not reaching saturation and the MO concentration was certain during the adsorption process with the increase of the adsorbent dose.

3.4.4. Effect of ionic strength

High concentration of salt may exist in the actual organic dye wastewater, and the presence of salt in water may affect the adsorption of organic dye by porous carbon. Therefore, the adsorption property of WWR-800 on the removal of MO was studied for a range of NaCl ionic strengths going from 0.05 to 0.5 M (Tan *et al.* 2016). It can be seen that the adsorption capacity decreased slightly with increasing concentration of NaCl (Figure 5(d)). The presence of electrolyte may cause the neutralization of the surface charge of the adsorbent while competing with MO for surface adsorption. With the increasing ionic strength, the adsorption capacity decreased due to screening of the surface charges (Krika & Benlahbib 2014).

3.4.5. Adsorption kinetics

In order to investigate the mechanism of the adsorption process, pseudo-first and pseudo-second order kinetic models were used to fit the kinetic experimental data. In the adsorption kinetics experiment, the concentration of MO was 50 mg/L (50 mL), the concentration of adsorbent WWR-800 was 0.25 g/L, the reaction temperature was 25 °C, and a series of reaction time gradients were set from 0 to 120 min.

Pseudo-first order model (Sadeek *et al.* 2014):

$$\log(q_e - q_t) = \frac{-k_1}{2.303}t + \log q_e \tag{3}$$

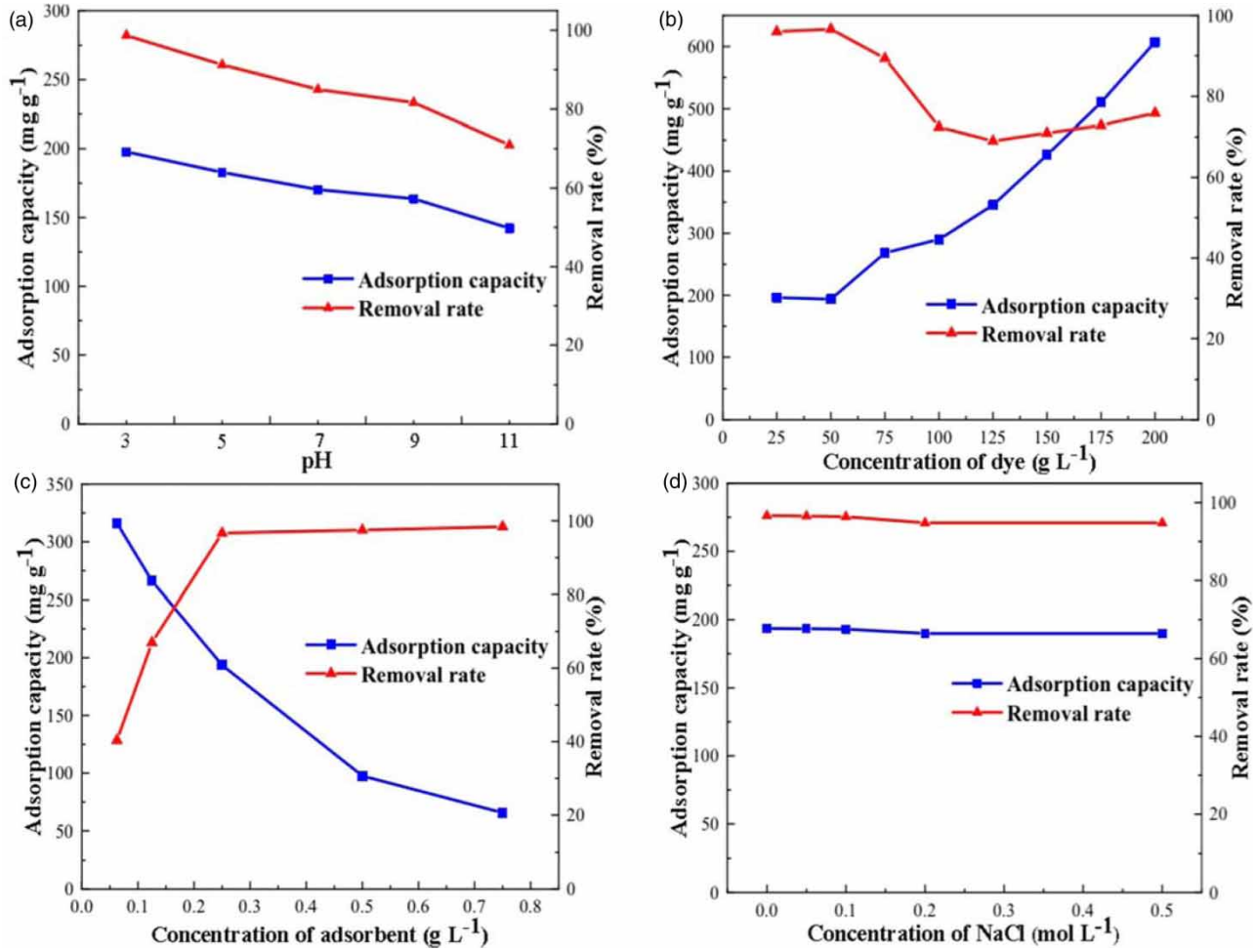

Figure 5 | (a) Influence of different pH. 50 mg/L of MO, 12.5 mg (0.25 g/L) of WWR-800, 25 °C; (b) influence of different concentrations of MO. Condition: 12.5 mg (0.25 g/L) of WWR-800, pH = 3, 25 °C; (c) influence of different dosing of WWR-800. Condition: 50 mg/L of MO, pH = 3, 25 °C; (d) influence of different ionic strengths. Condition: 50 mg/L of MO, 12.5 mg (0.25 g/L) of WWR-800, pH = 3, 25 °C.

Pseudo-second order model (Sadeek *et al.* 2014):

$$\frac{t}{q_t} = \frac{1}{q_e}t + \frac{1}{k_2 q_e^2} \tag{4}$$

where q_1 and q_2 are the amount of MO sorbed at equilibrium (mg g^{-1}), q_t is the amount of the MO sorbed at time t (mg g^{-1}), k_1 is the pseudo-first order equilibrium rate constant (min^{-1}), and k_2 is the pseudo-second order equilibrium rate constant (g mg^{-1} min).

The estimated kinetic parameters and coefficient of determination (R^2) from the pseudo-first order and pseudo-second order models are shown in Figure 6(a) and 6(b) and Table 2. The low R^2 value and the difference between experimental q_e and theoretical q_1 indicated that the pseudo-first order model was not well suited to describe the adsorption of MO by WWR-800. On the other hand, the R^2 value (0.999) for the pseudo-second order model was relatively higher than that of the pseudo-first order model. Moreover, the q_2 value (194.80 mg/g) calculated by the pseudo-second order model was close to the experimental q_e value (193.58 mg/g). Thus, these results suggested that the pseudo-second order model provided a good correlation for the adsorption of MO onto WWR-800.

3.4.6. Adsorption isotherms

The adsorption isotherm was the corresponding relationship curve between the equilibrium concentration and the equilibrium adsorption capacity. In the adsorption isotherm experiment, 50 mL MO solution with a series of concentrations

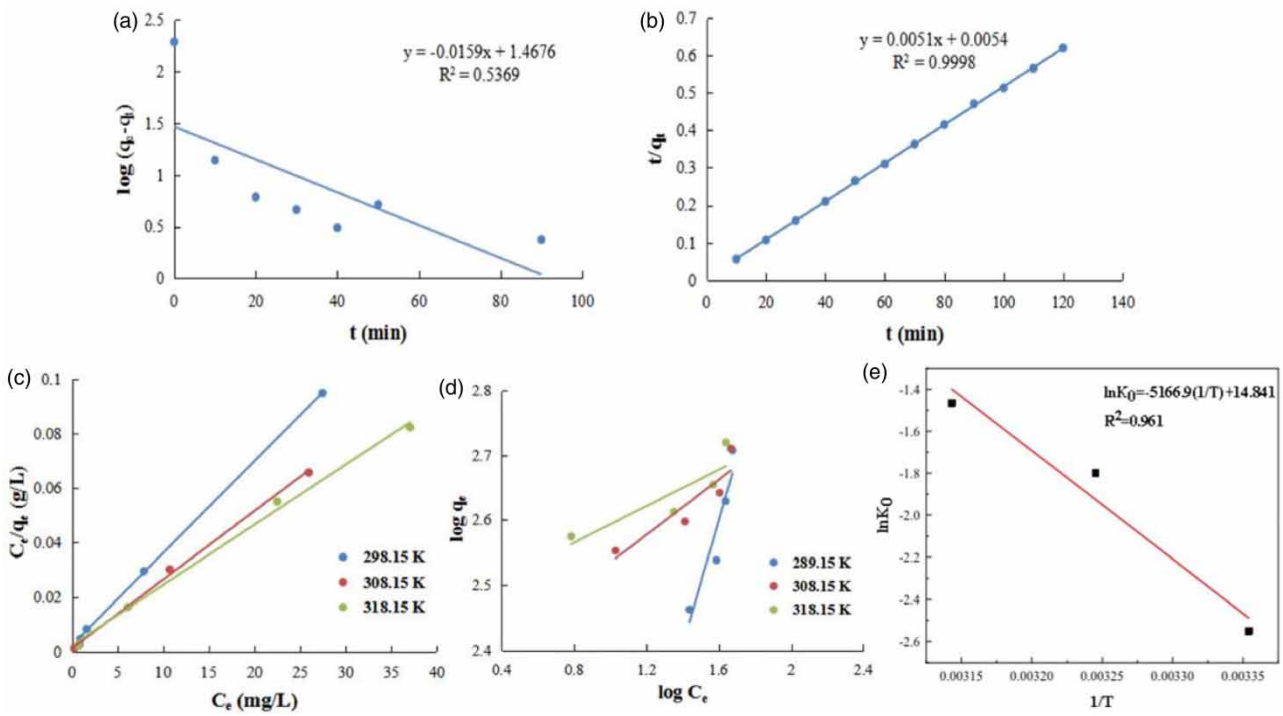

Figure 6 | (a) Pseudo-first order kinetic models fitting of MO by WWR-800; (b) pseudo-second order kinetic models fitting of MO by WWR-800; (c) Langmuir adsorption isotherms for adsorption of MO on WWR-800; (d) Freundlich adsorption isotherms for adsorption of MO on WWR-800 (e) Vant Hoff's plot for MO adsorption by WWR-800.

Table 2 | Fitting parameters of the adsorption kinetics models

Adsorption kinetic parameters						
	Pseudo-first order kinetic model			Pseudo-second order kinetic model		
q_e,exp/mg g^{-1}	q_e/mg g^{-1}	k_1	R^2	q_e/mg g^{-1}	k_2	R^2
193.58	29.35	0.037	0.537	196.08	0.005	0.999

gradients (25–200 mg/L) were set, the concentration of adsorbent WWR-800 was 0.25 g/L, and the adsorption time was 60 min. The commonly used adsorption isotherm models are the Langmuir and Freundlich models. The Langmuir model is based on the adsorption of a monolayer on the surface of the adsorbent, and the Freundlich model is based on the adsorption on a heterogeneous surface (Senthil Kumar *et al.* 2010). The obtained data for MO adsorption onto WWR-800 at 298.15, 308.15, and 318.15 K were fitted to Langmuir (Equation (5)) and Freundlich (Equation (6)) isotherms (Sadeek *et al.* 2014).

$$\frac{C_e}{q_e} = \frac{C_e}{q_L} + \frac{1}{k_L q_L} \tag{5}$$

where q_e (mg g^{-1}) is the MO uptake at equilibrium, q_L (mg g^{-1}) is the maximum MO uptake of WWR-800, and k_L (L mg^{-1}) is the constant related to the rate of adsorption.

$$\log q_e = \frac{\log C_e}{n} + \log k_F \tag{6}$$

where k_F (mg g^{-1}) and n indicate characteristic constants related to the relative sorption capacity of the sorbent and the intensity of sorption, respectively.

The results are summarized in Table 3, which showed the best fitting of the Langmuir model compared to the Freundlich model at the studied temperature (Figure 6(c) and 6(d)). It can be seen that the values of correlation coefficients of the Langmuir equation were higher than the Freundlich isotherm values, which indicated that the Langmuir isotherm correctly fitted the equilibrium data, confirming the mono-layer adsorption and supporting physisorption of MO molecules on the WWR-800 surface. Also, the value of equilibrium sorption capacity of the Langmuir equation (q_L) was more consistent with the experimental data than that of the Freundlich isotherm model. Therefore, the sorption reaction can be approximated more favorably by the Langmuir equation model.

Hence, we can find that some materials of adsorbent about MO (Table 4), such as commercially-activated carbon (AC) and porous carbons based on rice husk, pumpkin seed, wheat straw and so on (Su *et al.* 2013; Subbaiah & Kim 2016; Martini *et al.* 2018; Li *et al.* 2020). The adsorption capacity of MO on WWR-800 was relatively higher compared with the materials above. In addition, the adsorptive condition of MO on WWR-800 was accessible and the preparation of WWR-800 was simple, which indicated WWR-800 was an efficient, competitive and promising adsorbent for MO.

3.4.7. Adsorption thermodynamics

The determination of thermodynamics parameters had a great importance to evaluate spontaneity and heat change for the adsorption reactions. The free energy change (ΔG^0) of the adsorption reaction was given by the following equation (Sadeek *et al.* 2014):

$$\Delta G^0 = -RT \ln K_0 \tag{7}$$

where R is the universal gas constant (8.314×10^{-3} kJ mol^{-1}), T is the temperature in Kelvin (K) and K_0 is the sorption equilibrium constant determined from the slope of $\ln(q_e/C_e)$ against C_e at different temperatures (Jagtap *et al.* 2011).

Table 3 | Fitting parameters of the adsorption isotherm

Adsorption isothermal parameters

	Langmuir isotherm model			Freundlich isotherm model			
Temperature/K	q_L/mg g^{-1}	k_L	R^2	k_F/mg g^{-1}	n	R^2	q_e,exp/mg g^{-1}
298.15	294.12	1.42	0.999	11.36	1.04	0.883	290.06
308.15	400.00	2.08	0.998	209.70	4.70	0.825	396.12
318.15	454.55	0.92	0.996	283.60	7.11	0.765	451.65

Table 4 | MO sorption capacity by other materials

Adsorbent	q_m (mg g^{-1})	References
Wheat straw	50.4	Su *et al.* (2013)
Pumpkin seed	200.3	Subbaiah & Kim (2016)
Commercially-activated carbon(AC)	77.1	Martini *et al.* (2018)
Hollow molybdenum disulfide (h-MoS_2)	41.52	Wu *et al.* (2019)
Porous carbons based on rice husk	112	Li *et al.* (2020)
Aluminum hydroxide-bicarbonates	154	Kinoshita *et al.* (2020)
Lanthanum and cobalt sugar-based carbon	285.71	Liu *et al.* (2021)
Cubic magnetic $MgFe_2O_4$	535	Zhou *et al.* (2021)
WWR-800	454.55	This study

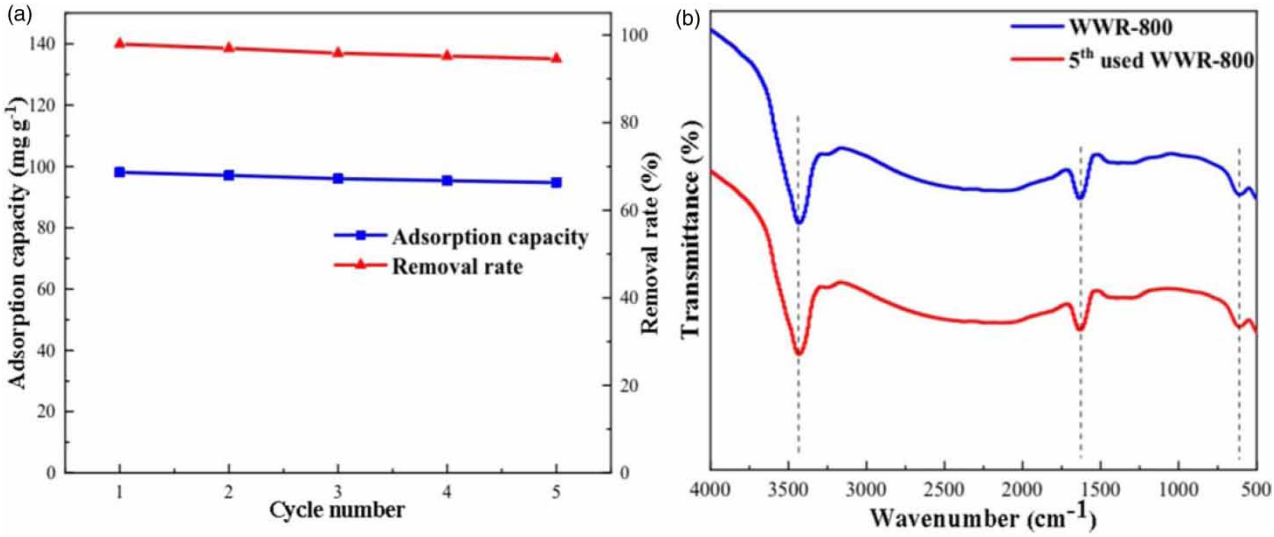

Figure 7 | (a) Adsorption of MO using the recycled adsorbent WWR-800; (b) FT-IR of the 5th used WWR-800. Condition: 50 mg/L of MO, 20 mg (0.5 g/L) of WWR-800, 25 °C.

The standard enthalpy change (ΔH^0), and standard entropy change (ΔS^0) were calculated using following equation (Sadeek *et al.* 2014):

$$\ln K_0 = -\frac{\Delta H^0}{RT} + \frac{\Delta S^0}{R} \tag{8}$$

where ΔH^0 is standard enthalpy change (kJ mol^{-1}) and ΔS^0 is standard entropy change (kJ mol^{-1} K^{-1}).

The values of ΔH^0 and ΔS^0 were obtained from the slope and intercept of the Van't Hoff's plot of lnK_0 against $1/T$ (Figure 6(c)). These were observed to be 42.96 kJ mol^{-1} and 0.1234 kJ mol^{-1} K^{-1}, respectively. The positive value of ΔH^0 for the process indicated that the adsorption of WWR-800 for MO was an endothermic process. The positive value of ΔS^0, which was a measure of randomness at the solid/liquid interface during MO sorption, indicated that the sorption process was irreversible and stable. The positive values of ΔG^0 6.32, 4.61, 3.87 kJ mol^{-1} at all temperatures studied indicated non-spontaneity of the sorption reaction under standard conditions (Mohammad *et al.* 2000).

3.4.8. Recyclability and stability of WWR-800

The recyclability and stability reusability of adsorbents were key factors in evaluating their potential applications because better repeated availability of adsorbents may reduce the overall cost of the adsorbent. Figure 7(a) showed the recycling of WWR-800 in the removal of MO. It can be clearly observed that the WWR-800 still possessed more than 94% adsorption capacities for MO even after five cycles of reuse. Besides, the 5th used adsorb had been characterized by FT-IR (Figure 7(b)). The chemical functional group of the 5th used WWR-800 retained the same stretching vibration as the fresh adsorbent. Among them, the absorption peak at 3,440 cm^{-1} may be the stretching vibration of hydroxyl (-OH), the absorption peak near 1,630 cm^{-1} may be formed by C = O stretching vibration of ketones or acids, and C=C stretching vibration of mononuclear aromatic hydrocarbons, and the absorption peak at 596 cm^{-1} was considered to be the stretching vibration of organic chloride (C-Cl). Taken together, these results indicated that WWR-800 provided good reusability and stability for MO adsorption.

4. CONCLUSION

In this study, we had demonstrated an easy and low-cost method to prepare wormwood rod-based porous carbons (WWRs). The adsorption properties of WWRs for the removal of MO from aqueous solution have been studied. Among all the adsorbents, the sample activated at 800 °C by NaCl (WWR-800) was found to exhibit the best adsorption performance. Several factors that affected the adsorption property were systematically explored under different conditions including solution pH, initial dye concentration, dosing of adsorbent and ionic strength. The kinetic data of the adsorption fitted well with

the pseudo-second-order kinetic model. At the same time, Langmuir and Freundlich isotherms were employed to describe the equilibrium adsorption, and the Langmuir model closely fitted the experimental data with better correlation coefficients. The maximum adsorption capacity of WWR-800 was 454.55 mg/g at 45 °C. Thermodynamic analyses revealed that the adsorption of MO on WWR-800 was endothermic and non-spontaneous. The present article was novel in terms of effective re-utilization of Chinese medicinal herbal residue as an inexpensive adsorbent candidate for dye removal.

ACKNOWLEDGEMENTS

The authors would like to acknowledge support from the science and technology innovation team plan for the youths in universities of Hubei province (T2020021) and Research Fund for Excellent Dissertation of China Three Gorges University.

AUTHOR STATEMENT

Shuhui Wang: Conceptualization, Methodology, Resources, Investigation, Data curation, Formal analysis, Writing-Original Draft, Writing-Review and Editing, Supervision and Proof reading.
Yu Huang: Conceptualization, Methodology, Formal analysis, Software.
Yiting Wu: Conceptualization, Methodology, Investigation.
Xinyu Zhang: Conceptualization, Methodology, Investigation.
Liu Wan: Resources, Writing-Reviewing and Editing, Supervision and Proof reading.
Xiang Liu: Resources, Supervision and Proof reading.
Wanju Zhang: Resources, Funding acquisition, Project administration, Supervision and Proof reading, Writing- Reviewing and Editing.

DECLARATION OF COMPETING INTEREST

The authors declare that they have no known competing financial interests or personal relationships that could have appeared to influence the work reported in this paper.

DATA AVAILABILITY STATEMENT

All relevant data are included in the paper or its Supplementary Information.

REFERENCES

Alatalo, S. M., Mäkilä, E., Repo, E., Heinonen, M., Salonen, J., Kukk, E., Sillanpää, M. & Titirici, M. M. 2016 Meso-and microporous soft templated hydrothermal carbons for dye removal from water. *Green Chem.* **18** (4), 1137–1146. https://doi.org/10.1039/C5GC01796C.

Anfruns, A., García-Suárez, E. J., Montes-Morán, M. A., Gonzalez-Olmos, R. & Martin, M. J. 2014 New insights into the influence of activated carbon surface oxygen groups on H_2O_2 decomposition and oxidation of pre-adsorbed volatile organic compounds. *Carbon* **77**, 89–98. https://doi.org/10.1016/j.carbon.2014.05.009.

Ayranci, E. & Duman, O. 2009 In-Situ UV-Visible spectroscopic study on the adsorption of some dyes onto activated carbon cloth. *Sep. Sci. Technol.* **44** (15), 3735–3752. http://dx.doi.org/10.1080/01496390903182891.

Azam, K., Raza, R., Shezad, N., Shabir, M., Yang, W., Ahmad, N., Shafiq, I., Akhter, P., Razzaq, A. & Hussain, M. 2020 Development of recoverable magnetic mesoporous carbon adsorbent for removal of methyl blue and methyl orange from wastewater. *J. Environ. Chem. Eng.* **8** (5), 104200. https://doi.org/10.1016/j.jece.2020.104220.

Bhatnagar, A., Sillanpää, M. & Witek-Krowiak, A. 2015 Agricultural waste peels as versatile biomass for water purification-a review. *Chem. Eng. J.* **270**, 244–271. https://doi.org/10.1016/j.cej.2015.01.135.

Cazetta, A. L., Pezoti, O., Bedin, K. C., Silva, T. L., Paesano Junior, A., Asefa, T. & Almeida, V. C. 2016 Magnetic activated carbon derived from biomass waste by concurrent synthesis: efficient adsorbent for toxic dyes. *ACS. Sustain. Chem. Eng.* **4** (3), 1058–1068. https://doi.org/10.1021/acssuschemeng.5b01141.

Gao, Y., Yue, Q., Gao, B. & Li, A. 2020 Insight into activated carbon from different kinds of chemical activating agents: a review. *Sci. Total. Environ.* **746**, 141094. https://doi.org/10.1016/j.scitotenv.2020.141094.

Ge, X., Tian, F., Wu, Z., Yan, Y., Cravotto, G. & Wu, Z. 2015 Adsorption of naphthalene from aqueous solution on coal-based activated carbon modified by microwave induction: microwave power effects. *Chem. Eng. Process.* **91**, 67–77.

Ghuge, S. P. & Saroha, A. K. 2018 Catalytic ozonation of dye industry effluent using mesoporous bimetallic Ru-Cu/SBA-15 catalyst. *Process. Saf. Environ.* **118**, 125–132. https://doi.org/10.1016/j.psep.2018.06.033.

Gokce, Y. & Aktas, Z. 2014 Nitric acid modification of activated carbon produced from waste tea and adsorption of methylene blue and phenol. *Appl. Surf. Sci.* **313**, 352–359. http://dx.doi.org/doi:10.1016/j.apsusc.2014.05.214.

Guo, L., Zhang, D., Xue, Z. J., Jiao, Q., Liu, A. P., Zheng, Y. G., Liu, E. H. & Duan, L. 2019 Comparison of *Artemisiae argyi* Folium and *Artemisiae lavandulaefoliae* Folium by simultaneous determination of multi-components with single reference standard method and chemometric analysis. *Phytochem. Anal.* **30** (1), 14–25. https://doi.org/10.1002/pca.2786.

Hu, J., Yu, H., Dai, W., Yan, X., Hu, X. & Huang, X. 2014 Enhanced adsorptive removal of hazardous anionic dye 'Congo red' by a Ni/Cu mixed-component metal-organic porous material. *RSC. Adv.* **4** (66), 35124–35130. https://doi.org/10.1039/C4RA05772D.

Hui, M., Shengyan, P., Ya, H., Rong, Z., Anatoly, Z. & Wei, C. 2018 A highly efficient magnetic chitosan 'fluid' adsorbent with a high capacity and fast adsorption kinetics for dyeing wastewater purification. *Chem. Eng. J.* **345**, 556–565. https://doi.org/10.1016/j.cej.2018.03.115.

Jager, D., Kupka, D., Vaclavikova, M., Ivanicova, L. & Gallios, G. 2018 Degradation of Reactive Black 5 by electrochemical oxidation. *Chemosphere* **190**, 405–416. https://doi.org/10.1016/j.chemosphere.2017.09.126.

Jagtap, S., Yenkie, M. K. N., Labhsetwar, N. & Rayalu, S. 2011 Defluoridation of drinking water using chitosan based mesoporous alumina. *Micropor. Mesopor. Mat.* **142** (2–3), 454–463. https://doi.org/10.1016/j.micromeso.2010.12.028.

Jain, S. N. & Gogate, P. R. 2019 Treatment of dye containing real industrial effluents using NaOH-activated *ficus racemosa* and *prunus dulcis* based novel adsorbents. *Int. J. Environ. Res.* **13** (2), 337–347. https://doi.org/10.1007/s41742-019-00179-8.

Katheresan, V., Kansedo, J. & Lau, S. Y. 2018 Efficiency of various recent wastewater dye removal methods: a review. *J. Environ. Chem. Eng.* **6** (4), 4676–4697. https://doi.org/10.1016/j.jece.2018.06.060.

Khanday, W. A. & Hameed, B. H. 2018 Zeolite-hydroxyapatite-activated oil palm ash composite for antibiotic tetracycline adsorption. *Fuel* **215**, 499–505. https://doi.org/10.1016/j.fuel.2017.11.068.

Kim, T. S., Song, H. J., Dar, M. A., Lee, H. J. & Kim, D. W. 2018 Fast adsorption kinetics of highly dispersed ultrafine nickel/carbon nanoparticles for organic dye removal. *Appl. Surf. Sci.* **439**, 364–370. https://doi.org/10.1016/j.apsusc.2018.01.061.

Kinoshita, Y., Shimoyama, Y., Masui, Y., Kawahara, Y., Arai, K., Motohashi, T., Noda, Y. & Uchida, S. 2020 Amorphous high surface area aluminum hydroxide-bicarbonates for highly-efficient methyl orange removal from water. *Langmuir* **36**, 6277–6285. https://doi.org/10.1021/acs.langmuir.0c00021.

Krika, F. & Benlahbib, O. F. 2014 Removal of methyl orange from aqueous solution via adsorption on cork as a natural and low-coast adsorbent: equilibrium, kinetic and thermodynamic study of removal process. *Desalin. Water. Treat.* **53** (13), 3711–3723. https://doi.org/10.1080/19443994.2014.995136.

Li, M., Liu, C., Cao, H., Zhao, H., Zhang, Y. & Fan, Z. 2014 KOH self-templating synthesis of three-dimensional hierarchical porous carbon materials for high performance supercapacitors. *J. Mater. Chem. A.* **2** (36), 14844–14851. https://doi.org/10.1039/C4TA02167C.

Li, D., Yang, Y., Li, C. & Liu, Y. 2017 A mechanistic study on decontamination of methyl orange dyes from aqueous phase by mesoporous pulp waste and polyaniline. *Environ. Res.* **154**, 139–144. http://dx.doi.org/10.1016/j.envres.2016.12.027.

Li, Y., Pan, B., Miao, H., Xu, H., Liu, X. & Shi, G. 2020 Single and binary dye adsorption of methylene blue and methyl orange in alcohol aqueous solution via rice husk based activated carbon: kinetics and equilibrium studies. *Chem. Res. Chinese. U.* **36** (6), 1272–1278. https://doi.org/10.1007/s40242-020-0063-9.

Liu, Q., Gao, Y., Zhou, N., Tian, G., Liang, N. & Dai, W. 2019 Highly improved water resistance and Congo red uptake capacity with a Zn/Cu-BTC@MC composite adsorbent. *J. Chem. Eng. Data* **64** (8), 3323–3330. https://doi.org/10.1021/acs.jced.9b00159.

Liu, X., Wu, Y. T., Ye, H. L., Chen, J., Xiao, W., Zhou, W. M. & Zaharaddeen, N. 2021 Modification of sugar-based carbon using lanthanum and cobalt bimetal species for effective adsorption of methyl orange. *Environ. Technol. Inno.* **23**, 101769. https://doi.org/10.1016/j.eti.2021.101769.

Lu, X., Liu, L., Yang, B. & Chen, J. 2009 Reuse of printing and dyeing wastewater in processess assessed by pilot-scale test using combined biological process and sub-filter technology. *J. Clean. Prod.* **17** (2), 111–114. https://doi.org/10.1016/j.apsusc.2018.01.061.

Martini, B. K., Daniel, T. G., Corazza, M. Z. & Carvalho, A. E. 2018 Methyl orange and tartrazine yellow adsorption on activated carbon prepared from boiler residue: kinetics, isotherms, thermodynamics studies and material characterization. *J. Environ. Chem. Eng.* **6** (5), 6669–6679. https://doi.org/10.1016/j.jece.2018.10.013.

Menya, E., Olupot, H., Storz, M. & Kiros, Y. 2018 Production and performance of activated carbon from rice husks for removal of natural organic matter from water: a review. *Chem. Eng. Res. Des.* **129**, 271–296. https://doi.org/10.1016/j.cherd.2017.11.008.

Mohammad, A., Rifaqat, A. K. L., Rais, A. & Jameel, A. 2000 Adsorption studies on *citrus reticulata* (fruit peel of orange): removal and recovery of Ni(II) from electroplating wastewater. *J. Hazard. Mater.* **79**, 117–131. https://doi.org/10.1016/S0304-3894(00)00234-X.

Mohan, D., Sarswat, A., Ok, Y. S. & Pittman, C. U. 2014 Organic and inorganic contaminants removal from water with biochar, a renewable, low cost and sustainable adsorbent-a critical review. *Bioresour. Technol.* **160**, 191–202. http://dx.doi.org/10.1016/j.biortech.2014.01.120.

Qian, W., Zhu, J., Zhang, Y., Wu, X. & Yan, F. 2015 Condiment-derived 3D architecture porous carbon for electrochemical supercapacitors. *Small* **11** (37), 4959–4969. https://doi.org/4959-69. 10.1002/smll.201500859.

Sadeek, A. S., Mahmoud, O. A., Mohamed, A. E. & Maisa, M. A. 2014 Selective solid-phase extraction of U(VI) by amine functionalized glycidyl methacrylate. *J. Eeviron. Chem. Eng.* **2**, 293–303. http://dx.doi.org/10.1016/j.jece.2013.12.015.

Saleh, T. A. 2018 Simultaneous adsorptive desulfurization of diesel fuel over bimetallic nanoparticles loaded on activated carbon. *J. Clean. Prod.* **172**, 2123–2132. https://doi.org/10.1016/j.jclepro.2017.11.208.

Saleh, T. A., Sulaiman, K. O., Al-Hammadi, S. A., Dafalla, H. & Danmaliki, G. I. 2017 Adsorptive desulfurization of thiophene, benzothiophene and dibenzothiophene over activated carbon manganese oxide nanocomposite: with column system evaluation. *J. Cleaner Prod.* **154**, 401–412. https://doi.org/10.1016/j.jclepro.2017.03.169.

Senthil Kumar, P., Ramalingam, S., Senthamarai, C., Niranjanaa, M., Vijayalakshmi, P. & Sivanesan, S. 2010 Adsorption of dye from aqueous solution by cashew nut shell: studies on equilibrium isotherm, kinetics and thermodynamics of interactions. *Desalination* **261** (1-2), 52–60. https://doi.org/10.1016/j.desal.2010.05.032.

Su, Y., Jiao, Y., Dou, C. & Han, R. 2013 Biosorption of methyl orange from aqueous solutions using cationic surfactant-modified wheat straw in batch mode. *Desalin. Water. Treat.* **52** (31–33), 6145–6155. https://doi.org/10.1080/19443994.2013.811121.

Subbaiah, M. V. & Kim, D. S. 2016 Adsorption of methyl orange from aqueous solution by aminated pumpkin seed powder: kinetics, isotherms, and thermodynamic studies. *Ecotoxicol. Environ. Saf.* **128**, 109–117. https://doi.org/10.1016/j.ecoenv.2016.02.016.

Sun, L., Yuan, D., Wan, S., Yu, Z. & Dang, J. 2018 Adsorption performance and mechanisms of methylene blue removal by non-magnetic and magnetic particles derived from the *vallisneria natans* waste. *J. Polym. Environ.* **26** (7), 2992–3004. https://doi.org/10.1007/s10924-018-1185-8.

Tan, X., Liu, S., Liu, Y., Gu, Y., Zeng, G., Cai, X., Yan, Z., Yang, C., Hu, X. & Chen, B. 2016 One-pot synthesis of carbon supported calcined-Mg/Al layered double hydroxides for antibiotic removal by slow pyrolysis of biomass waste. *Sci. Rep.* **6**, 39691. https://doi.org/10.1038/srep39691.

Toumi, K. H., Benguerba, Y., Erto, A., Dotto, G. L., Khalfaoui, M., Tiar, C., Nacef, S. & Amrane, A. 2018 Molecular modeling of cationic dyes adsorption on agricultural Algerian olive cake waste. *J. Mol. Liq.* **264**, 127–133. https://doi.org/10.1016/j.molliq.2018.05.045.

Wang, Y., Liu, Y., Liu, W., Zhang, G., Liu, G., Chen, H. & Yang, J. L. 2016 Large-scale synthesis of highly porous carbon nanosheets for supercapacitor electrodes. *J. Alloy. Compd.* **677**, 105–111. http://dx.doi.org/10.1016/j.jallcom.2016.03.232.

Wang, C., Wu, D., Wang, H., Gao, Z., Xu, F. & Jiang, K. 2018 A Green and scalable route to yield porous carbon sheets from biomass for supercapacitors with high capacity. *J. Mater. Chem. A.* **6** (3), 1244–1254. https://doi.org/10.1039/c7ta07579 k.

Wang, Z., Wang, K., Wang, Y., Wang, S., Chen, Z., Chen, J. & Fu, J. 2019 Large-scale fabrication of N-doped porous carbon nanosheets for dye adsorption and supercapacitor applications. *Nanoscale* **11** (18), 8785–8797. https://doi.org/10.1039/x0xx00000x.

Wei, X. J., Li, Y. B. & Gao, S. Y. 2017 Biomass-derived interconnected carbon nanoring electrochemical capacitors with high performance in both strongly acidic and alkaline electrolytes. *J. Mater. Chem. A.* **5**, 181–188. https://doi.org/ 10.1039/c7ta90196h.

Wong, S., Ngadi, N., Inuwa, I. M. & Hassan, O. 2018 Recent advances in applications of activated carbon from biowaste for wastewater treatment: a short review. *J. Clean. Prod.* **175**, 361–375. https://doi.org/10.1016/j.jclepro.2017.12.059.

Wu, Y. H., Sua, M., Chen, J. W., Xu, Z. P., Tang, J. F., Chang, X. Y. & Chen, D. Y. 2019 Superior adsorption of methyl orange by h-mos_2 microspheres: isotherm, kinetics, and thermodynamic studies. *Dyes. Pigments* **170**, 107591. https://doi.org/10.1016/j.dyepig.2019.107591.

Xia, J. X., Zhao, B. B., Zan, J. F., Wang, P. & Chen, L. L. 2019 Simultaneous determination of phenolic acids and flavonoids in *Artemisiae Argyi* Folium by HPLC-MS/MS and discovery of antioxidant ingredients based on relevance analysis. *J. Pharm. Biomed. Anal.* **175**, 112734. https://doi.org/10.1016/j.jpba.2019.06.031.

Yang, Y., Xie, Y., Pang, L., Li, M., Song, X., Wen, J. & Zhao, H. 2013 Preparation of reduced graphene oxide/poly(acrylamide) nanocomposite and its adsorption of Pb(II) and methylene blue. *Langmuir* **29** (34), 10727–10736. https://doi.org/10.1021/la401940z.

Yao, L., Yang, J., Zhang, P. & Deng, L. 2018 In situ surface decoration of $Fe_3C/Fe_3O_4/C$ nanosheets: towards bi-functional activated carbons with supercapacitance and efficient dye adsorption. *Bioresour. Technol.* **256**, 208–215. https://doi.org/10.1016/j.biortech.2018.02.027.

Yeap, K. L., Teng, T. T., Poh, B. T., Morad, N. & Lee, K. E. 2014 Preparation and characterization of coagulation/flocculation behavior of a novel inorganic-organic hybrid polymer for reactive and disperse dyes removal. *Chem. Eng. J.* **243**, 305–314. https://doi.org/10.1016/j.cej.2014.01.004.

Yu, M., Han, Y., Li, J. & Wang, L. 2017 CO_2-activated porous carbon derived from cattail biomass for removal of malachite Green dye and application as supercapacitors. *Chem. Eng. J.* **317**, 493–502. http://dx.doi.org/10.1016/j.cej.2017.02.105.

Zereshki, S., Daraei, P. & Shokri, A. 2018 Application of edible paraffin oil for cationic dye removal from water using emulsion liquid membrane. *J. Hazard. Mater.* **356**, 1–8. https://doi.org/10.1016/j.jhazmat.2018.05.037.

Zhang, B., Song, C., Liu, C., Min, J., Azadmanjiri, J., Ni, Y., Niu, R., Gong, J., Zhao, Q. & Tang, T. 2019 Molten salts promoting the 'controlled carbonization' of waste polyesters into hierarchically porous carbon for high-performance solar steam evaporation. *J. Mater. Chem. A.* **7** (40), 22912–22923. https://doi.org/10.1039/C9TA07663H.

Zhao, S., Chen, F., Zhu, X., Liu, W., Wu, C., Zhang, J., Ren, S., Yan, Z., Cao, W., Zhang, Q. & Li, X. 2021 An azine-based polymer derived hierarchically porous N-doped carbon for hydrophilic dyes removal. *J. Hazard. Mater.* **413**, 125299. https://doi.org/10.1016/j.jhazmat.2021.125299.

Zhou, L. Y., Liu, J. X., Lu, A. M., Shen, J. N., Xu, J. Y. & Jiang, H. M. 2021 Controllable synthesis of cubic magnetic $MgFe_2O_4$ derived from MgFe-LDHs for efficient removal of Methyl orange. *Chem. Eng. J.* **428**, 131174. https://doi.org/10.1016/j.cej.2021.131174.

First received 2 August 2021; accepted in revised form 2 October 2021. Available online 14 October 2021